SUPPLEMENTAL INFORMATION

Sodium channel *SCN3A* (Nav1.3) regulation of human cerebral cortical folding and oral motor development

Richard S. Smith, Connor J. Kenny, Vijay Ganesh, Ahram Jang, Rebeca Borges-Monroy, Jennifer N. Partlow, R. Sean Hill, Taehwan Shin, Allen Y. Chen, Ryan N. Doan, Anna-Kaisa Anttonen, Jaakko Ignatius, Livija Medne, Carsten G. Bönnemann, Jonathan L. Hecht, Oili Salonen, A. James Barkovich, Annapurna Poduri, Martina Wilke, Marie Claire Y. de Wit, Grazia M.S. Mancini, Laszlo Sztriha, Kiho Im, Dina Amrom, Eva Andermann, Ritva Paetau, Anna-Elina Lehesjoki, Christopher A. Walsh, and Maria K. Lehtinen

Figure S1

Mapping and sequencing of Families A-F *SCN3A* pathogenic variants; Related to Figure 1

Table S1

Phenotypic descriptions of affected individuals in Family A; Related to Figure 1

Table S2

Detailed electrophysiological data of sodium currents recorded from *SCN3A*-WT, *SCN3A*-F1759Y, or *SCN3A*-I875T expressing cells; Related to Figure 2

Figure S2

Overexpression of *SCN3A* in human fetal cortical neurons stimulates neurite branching, and this effect is attenuated in *SCN3A* mutants; Related to Figure 2

Figure S3

Analysis of *SCN3A* expression in fetal and adult human cortex; Related to Figure 3

Figure S4

In utero overexpression of *SCN3A* harboring a pathogenic mutation causes atypical cortical development in the gyrencephalic ferret; Related to Figure 4

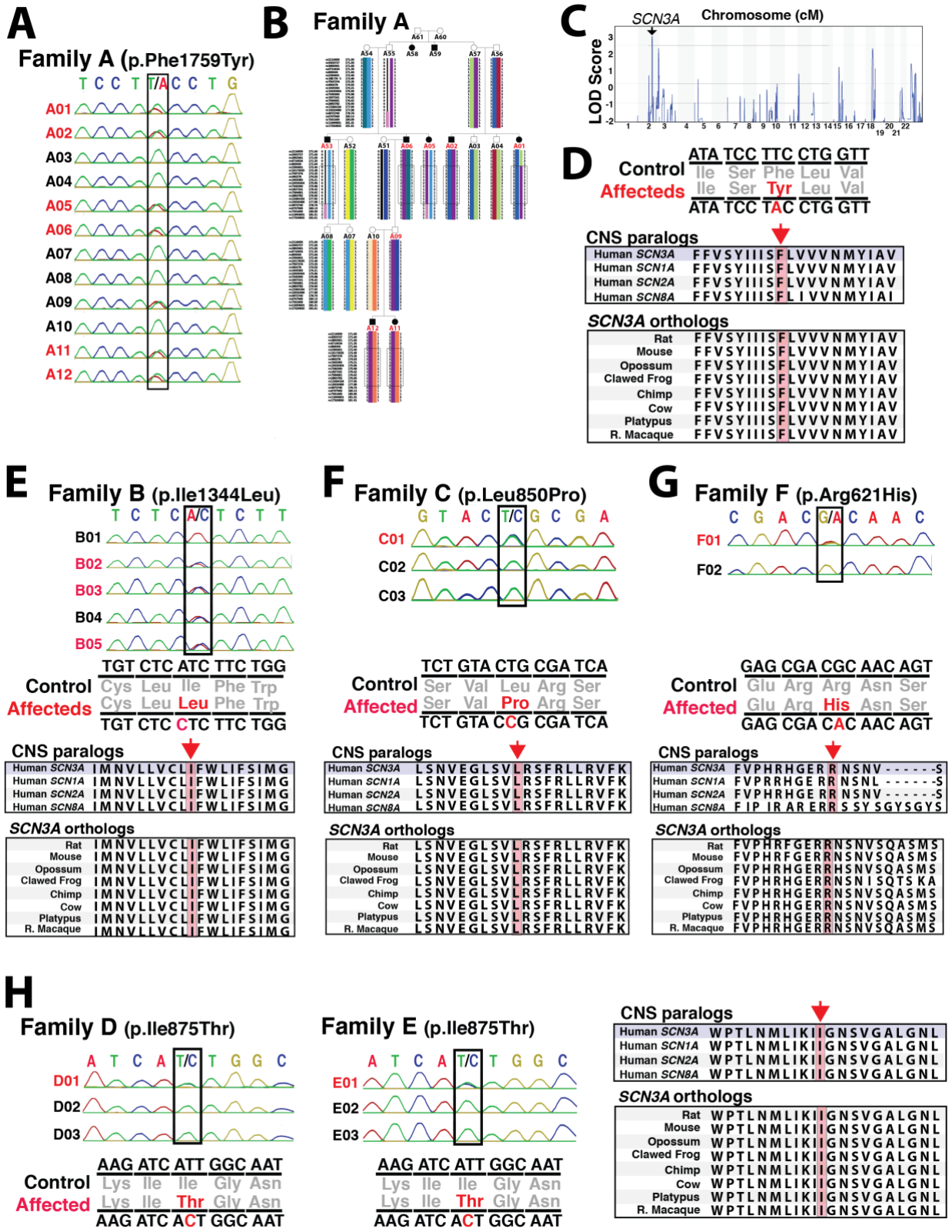

Figure S1 Mapping and sequencing of *SCN3A* (Nav1.3) mutations; Related to Figure 1

Figure S1. Mapping and sequencing of *SCN3A* (Nav1.3) pathogenic variants; Related to Figure 1

(A) Representative *SCN3A* Sanger chromatograms from unaffected (black text) and affected (red text) individuals of Family A. Affected individuals have a heterozygous T>A substitution. **(B)** Haplotype mapping of Family A. **(C)** Plot of LOD score from genome-wide multipoint linkage analysis using data from the Illumina Infinium HumanHap550-Duo BeadChip of Family A; arrow indicates *SCN3A* location at maximum LOD score of 2.48. **(D)** Sequence alignment of the amino acids surrounding the Family B mutation from CNS Nav isoforms and orthologs across species, showing high degree of conservation. **(E)** Representative *SCN3A* Sanger chromatograms from unaffected and affected individuals of Family B. The affected individual has a heterozygous A>C substitution. *Bottom,* Sequence alignment of the amino acids surrounding the Family B mutation from CNS Nav isoforms and orthologs across species, showing high degree of conservation. **(F-H)** Representative *SCN3A* Sanger chromatograms from unaffected and affected individuals of Families C, D, E, and F. *Bottom,* Sequence alignment of the amino acids surrounding the Families C, D, E, and F mutation from CNS Nav isoforms and orthologs across species, showing high degree of conservation.

Subject	A01	A02	A05	A11	A12
Ages when studied	68 - 69 years	56 - 57 years	70 years	6-30 years	4-28 years
Gross motor abilities	Normal	R. Hemiplegia	Skilled	Normal	Normal
Finger movement	Clumsy	Clumsy	Normal	Normal	Clumsy
Horizontal tongue movement	Absent	Absent	Absent	Absent to R	Absent
Speech	Dysarthria, Vocal speech	Dysarthria, Vocal speech	Dysarthria, Jargon	Dysarthria, Intelligible	Dysarthria, Vocal speech
Intellectual Disability (ID)	Mild ID	Mild ID	Moderate ID	Borderline ID	Borderline ID
VIQ	NA	50	NA, AAgn	73	62
PIQ	NA	73	15	88	85
FSIQ	NA	58	NA	79	71
Epilepsy	No	No	No	No	One seizure
EEG or MEG	Occipital spikes	Low amplitudes L. posterior	Normal	Rolandic spikes at 6 – 8 years	ESES at 4 -13 years
Cortical AER	Normal	NA	NA	Normal	Normal
Cortical SER	Normal	Normal	Normal	Normal	Normal
Independent living	Yes	Yes	No	Yes	Yes

Table S1. Phenotype descriptions of affected individuals in Family A; Related to Figure 1

Supplemental Table 1. Phenotypic descriptions of affected individuals in Family A; Related to Figure 1

VIQ = Verbal Intelligence Quotient, PIQ = Performance Intelligence Quotient, FSIQ = Full-Scale Intelligence Quotient, EEG = Electroencephalogram, MEG = Magnetoencephalogram, AER = Auditory Evoked Response, SER = Somatosensory Evoked Response, ID = Intellectual disability, NA = not available, AAgn = auditory agnosia, ESES = Electrical Status Epilepticus in Sleep, L. = left, R. = right.

Mean	*SCN3A*-WT (N=33)	*SCN3A*-F1759Y (n=28)	*SCN3A*-I875T (n=17)
$V_{1/2}$ (mV)	-20.5 ± 1.4	-12.7 ± 0.9 **	-25.9 ± 2.4 **
I_{peak} (pA/pF)	435 ± 45	292 ± 27 *	136 ± 14 **
I-Na_P (%)	22 ± 2.9	60 ± 12 **	32 ± 2.7 *
SS-I $V_{1/2}$ (mV)	-40 ± 2.7	-35.2 ± 2.4	-35.5 ± 3.1
SS-I Slope	12.7 ± 2.8	10.2 ± 2.6	16.3 ± 3.4
Area (nA/pF x ms)	46.3 ± 5.3	74.6 ± 9.9 *	12.9 ± 1.1 **

Table S2. Detailed electrophysiological data of sodium currents recorded from *SCN3A*-WT, *SCN3A*-F1759Y, *SCN3A*-I875T expressing cells; Related to Figure 2

Table S2. Detailed electrophysiological data of sodium currents recorded from *SCN3A*-WT, *SCN3A*-F1759Y, and *SCN3A*-I875T expressing cells; Related to Figure 2

SCN3A is coexpressed with β1 and β2 auxiliary subunits to support channel function and membrane localization (Hull and Isom, 2017). $V_{1/2}$: Voltage-dependence of activation describes the potential which 50% of sodium channels are active, and determined by curve fitting. SS-$V_{1/2}$ describes the potential which 50% of sodium channels are inactivated (steady state), and determined by curve fitting. Since mutant channels (I875T and F1759Y) exhibited increased non-inactivating currents during the pre-pulse, statistics were calculated at WT channels SS-$V_{1/2}$ (F1759Y and I875T; $p = 0.23$, $n = 28$; and $p = 0.27$, $n=17$; respectively; t-test, $*p < 0.05$; $**p < 0.01$). I_{peak} (pA/pF) is the maximal inward current detected in a neuron and normalized to the whole cell capacitance. I-Na_P (%) describes the non-inactivating persistent current following activation, measured as mean of last 30ms of voltage step and presented as a percentage of the peak current. Area (nA/pF x ms) represents measurement of current density.

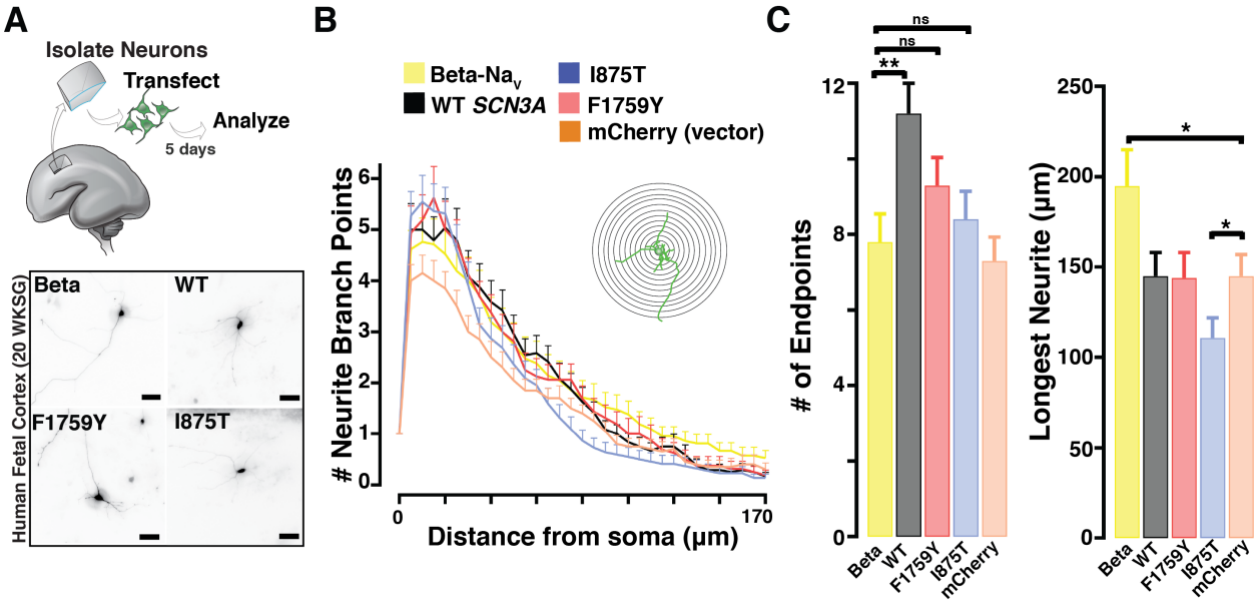

Figure S2 Overexpression of *SCN3A* in human fetal cortical neurons stimulates neurite branching, and this effect is attenuated in *SCN3A* mutants; Related to Figure 2

Figure S2. Overexpression of *SCN3A* in human fetal cortical neurons stimulates neurite branching, and this effect is attenuated in *SCN3A* mutants; Related to Figure 2

(A) *Upper panels,* Experimental design showing strategies employed on human (20 WKSG) cortical neurons. Dissociated cortical neurons were transfected with *SCN3A* prior to seeding (day 0) and cultured for 5 days. *Lower panels,* Fluorescence images of human cortical neurons transfected with mCherry together with GFP-β-Nav, *SCN3A*-WT, -F1759Y, or -I875T expression vectors. Scale bar, 50 µm. **(B)** Cortical neurons transfected with mCherry together with GFP-β-Nav, *SCN3A*-WT, -F1759Y, or -I875T expression vectors were analyzed for neurite complexity using Sholl analysis. Graph displays neurite complexity as quantified by the number of neurite branches a single neuron has in increasing distance from the cell soma. *Top right,* camera lucida drawing of a representative cortical neuron (green) and neurites crossing over superimposed concentric circles (10 µm per step) used for Sholl analysis (range from 10 µm to 120 µm from the center of the neuronal soma). **(C)** Histograms showing number of branch endpoints per neuron show that *SCN3A* transfection increases neurite complexity, and this effect was attenuated by I875T and F1759Y mutations (*left*; WT, 11.2 ± 0.8, n=35; vs Nav-Beta, 7.8 ± 0.76, n = 33, t-test, p = 0.003; WT, 11.2 ± 0.8, n=35; vs I875T, 8.4 ± 0.75, n = 38, t-test, p = 0.012; WT, vs. mCherry, 7.3 ± 0.63, n=31, t-test, p = 0.0004; mCherry, vs. F1759Y, 9.3 ± 0.74 mV, n = 30, t-test, p = 0.04). The longest neurite was not greatly affected by WT-*SCN3A* but modestly impaired by the I875T mutation (*right;* in microns, mCherry, 145.2 ± 11.9, n = 31; mCherry, vs. I875T, 111 ± 11, n = 38, t-test, p = 0.038; mCherry, vs. Nav-beta, 195 ± 20, n = 33, t-test, p = 0.039; mCherry, vs. F1759Y, 144 ± 14, n = 30, t-test, p = 0.94) in neurons transfected with Nav–Beta (yellow), *SCN3A*-WT (black), *SCN3A*-F1759Y (red), or *SCN3A*-I875T (blue), mCherry vector (orange). Measurements presented as mean ± S.E.M, with n = 30–40 neurons per experimental condition; t-test, *p < 0.05, **p < 0.02.

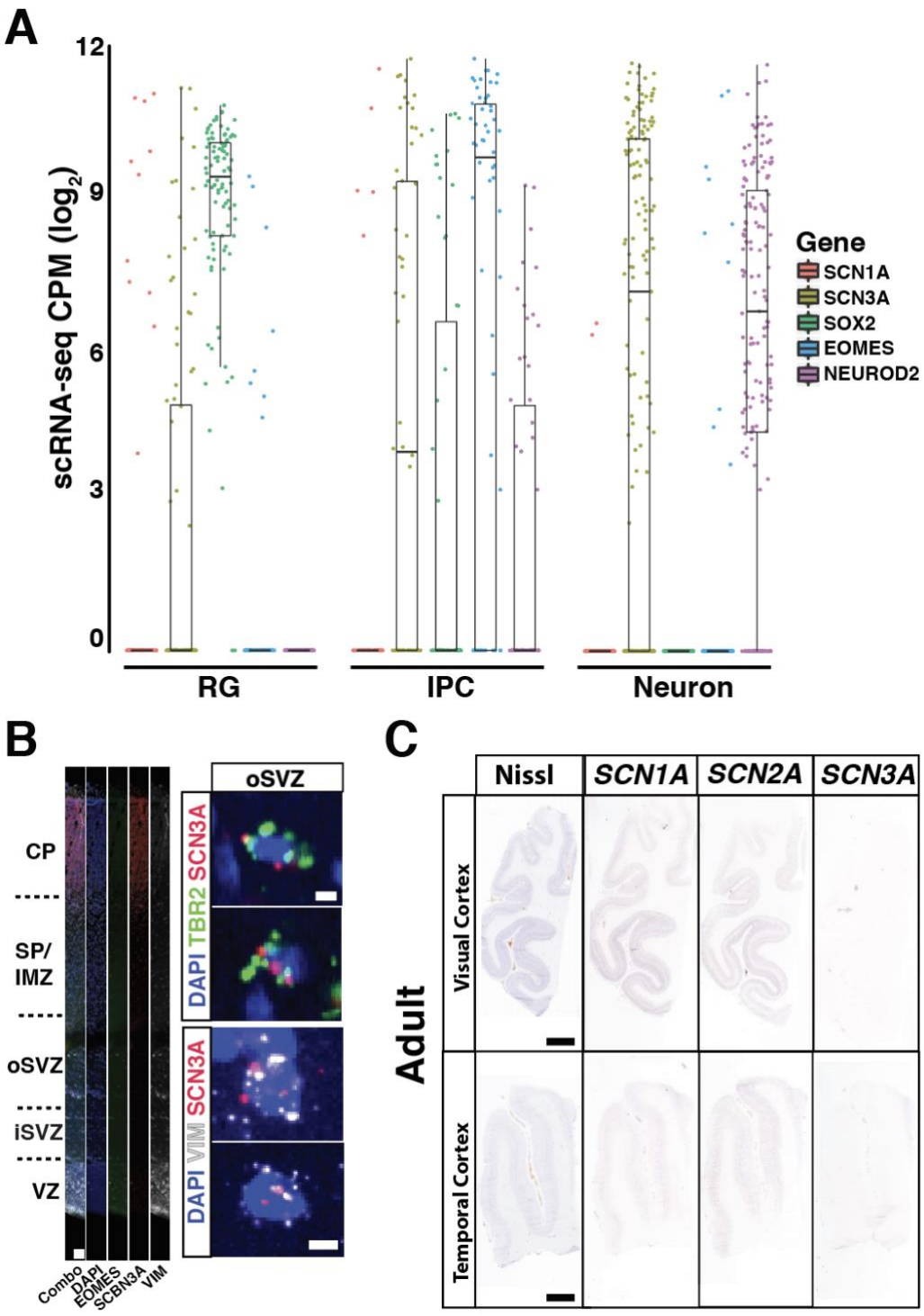

Figure S3. Analysis of sodium channel subtypes in the fetal and adult human cortex; Related to Figure 3

Figure S3. Analysis of sodium channel subtypes in fetal and adult human cortex; Related to Figure 3

(A) Single cell RNA-seq dataset generated from 16-18 WKSG fetal cortex (Pollen et al., 2015) and clustered into specific cell types (RGC, radial glial cell; IPC, intermediate progenitor cell; neuron, excitatory neuron). Graphs include cell type specific markers (RGC marker *SOX2*, IPC marker *EOMES* [*TBR2*], and neuronal marker *NEUROD2*). Graph in RNA Counts per million, CPM (Log2). Statistics demonstrating *SCN3A* enriched compared to *SCN1A* across all cell types: RGCs ($p < 0.005$), IPCs ($p < 0.001$), and neurons ($p < 0.001$). **(B)** Multiplex mRNA *in situ* at 20 WKSG show highest *SCN3A* expression in the human cortical plate (CP), and to a lesser extent, the ventricular zone (VZ), suggesting that *SCN3A* has roles in neurons and neural progenitors. Cell type specific markers for intermediate progenitors (TBR2) and neural progenitors (Vimentin, VIM) show *SCN3A* transcripts present in oSVZ. Scale bar left, 100µm and right, 5µm. **(C)** RNA *in situ* for *SCN1A, SCN2A, SCN3A* transcripts in adult human temporal and visual cortices demonstrate varying levels of gene expression (male, 46 years, left hemisphere, ABA). Scale bar, 1mm. ISH data from (C) was generated from the ABA.

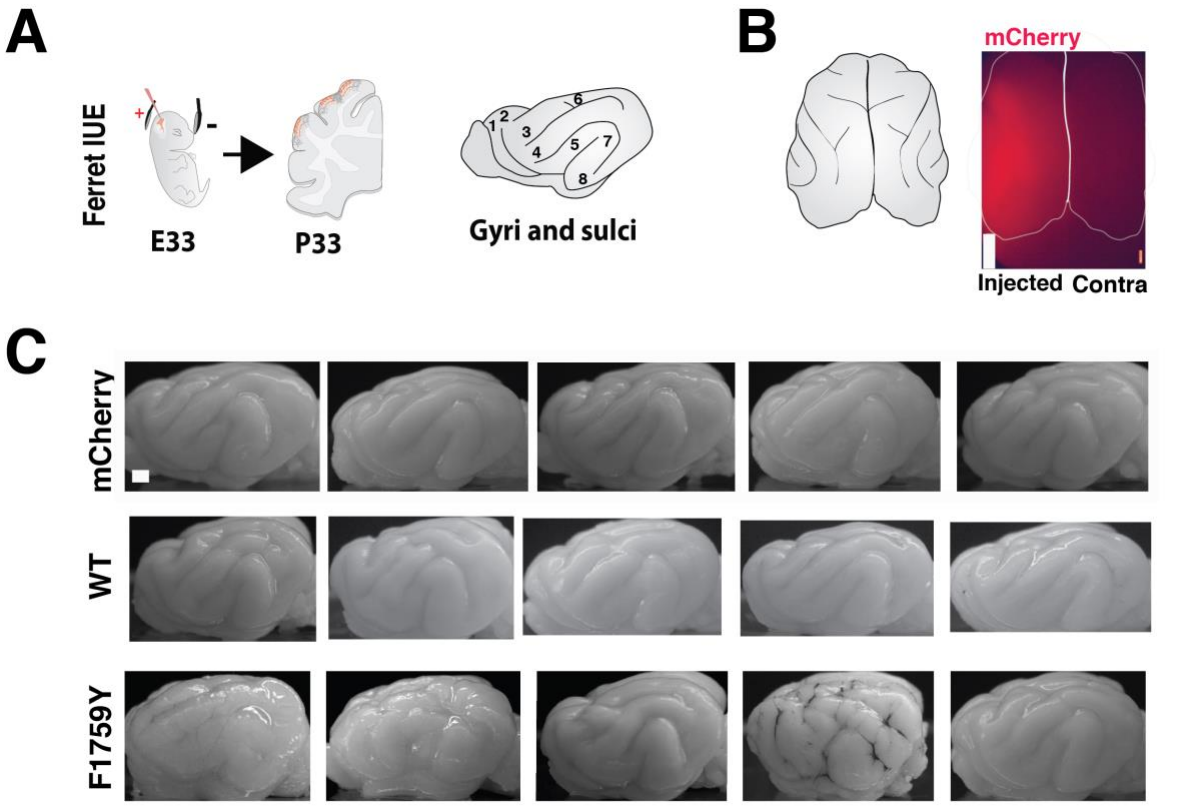

F

		Vector	*SCN3A*	F1759Y
	Bin	n=195	n=177	n=187
CP	1	74.6 ± 3.6	66.6 ± 4.5	38.6 ± 2.5 **
	2	11.5 ± 1.1	9.4 ± 0.3	4.7 ± 0.5**
	3	6.5 ± 1.2	7 ± 1.8	9.4 ± 1.1
	4	4.1 ± 0.9	3.3 ± 0.4	17.7 ± 2.3 **
VZ	5	3 ± 0.7	13.3 ± 1.8 **	29.7 ± 11**

Figure S4. *In utero* overexpression of pathogenic *SCN3A* causes atypical cortical development in the gyrencephalic ferret; Related to Figure 4

Figure S4. *In utero* overexpression of pathogenic *SCN3A* causes atypical cortical development in the gyrencephalic ferret; Related to Figure 4

(A) Experimental schematic for IUE and tissue collection performed as in Figure 4A, with horizontal anatomical profile of the stereotyped ferret gyri/sulci at ~33 postnatal days (P33). **(B)** Epifluorescence image of a mCherry positive cortical hemisphere after IUE. Scale bar, 3mm. **(C)** Images of ~P33 old ferret electroporated with *SCN3A*-WT, pathogenic variant (*SCN3A*-F1759Y), and mCherry control. Scale bar, 3mm. Sagittal view of the ferret brain, indicating the names of the main cortical gyri; 1. Orbital gyrus, 2. Anterior sigmoid gyrus, 3. Posterior sigmoid gyrus, 4. Coronal gyrus, 5. Lateral gyrus, 6. Ectosylvian gyrus. 7. Supra-sylvian gyrus. **(D)** Coronal brain section from *SCN3A*-F1759Y at P15 with antibody staining for upper cortical layer marker SATB2, deep-layer maker CTIP2, and mCherry positive cells. Arrow denotes a change in SATB2-positive staining cell density around *SCN3A*-positive electroporated area, but CTIP2 was unaffected, suggesting a cell non-autonomous effect during later stages of cortical lamination. Scale bar, 400μm. Black spaces present within tissue occur sometimes during cryopreservation and sectioning. **(E)** Coronal brain section at P30 showing *SCN3A*-F1759Y IUE with antibody staining for upper cortical layer marker SATB2 (yellow) and *SCN3A*-F1759Y mCherry positive cells and processes (red). White arrow marks a grouping of misplaced SATB2 positive cells surrounded by mCherry neurites. Scale bar, 500μm. **(F)** Data table from Figure 4D, showing distribution of cells across assigned cortical bins. Student's t-test * $p < 0.05$, ** $p < 0.01$.